Electric Power Systems Research 190 (2021) 106706

Contents lists available at ScienceDirect

Electric Power Systems Research

journal homepage: www.elsevier.com/locate/epsr

Operational reliability assessment of photovoltaic inverters considering voltage/VAR control function

Qingmian Chai[a], Cuo Zhang[a,*], Zhao Yang Dong[a], Yan Xu[b]

[a] School of Electrical Engineering and Telecommunications, The University of New South Wales, Sydney, NSW 2052, Australia
[b] School of Electrical and Electronic Engineering, Nanyang Technological University, 639798, Singapore

ARTICLE INFO

Keywords:
Active distribution networks
Photovoltaics
Reliability analysis
Uncertainty
Voltage/VAR control

ABSTRACT

This paper proposes an operational reliability assessment approach of photovoltaic (PV) inverters considering a voltage/VAR control (VVC) function. The approach aims to quantify the reliability degradation and estimate the lifetime of PV inverters when they are utilized for the VVC function. Firstly, an inverter based VVC model considering uncertain profiles of PV power generation and loads is developed and it is solved by a stochastic optimization method. Then, a long-term reliability assessment procedure of the inverters utilized in the VVC model is proposed. To assess the reliability, a power loss model considering the VVC results is developed and a modified lifetime model based on Coffin-Manson model and manufacturing information is proposed. The proposed VVC model and inverter reliability assessment approach are verified on a 33-bus distribution network. The simulation results reveal the long-term impacts of additional utilization in the VVC function on operational reliability and lifetime of PV inverters.

1. Introduction

1.1. Photovoltaic development and ancillary services

Solar energy is considered as a primary alternative energy resource to reduce the reliance on traditional fossil energy. With the advance of modern technologies, the utilization of photovoltaics (PVs) has been in a rapid growth in the power systems. It is reported by [1] that there are over 2 million distributed rooftop PV systems installed in Australia. The distributed PVs that significantly penetrate in distribution networks can be aggregated as virtual power plants (VPPs), which can provide reliable management support for the power systems. Moreover, the PV based VPPs have the potential to support ancillary services such as voltage/VAR control (VVC) functions. IEEE 1547.8 working group has been revising relevant standards to allow PV inverters to participate in network voltage regulation [2]. Electric Power Research Institute [3] has recently given protocols for inverter based reactive power compensation methods, including various control modes. Furthermore, it is suggested that PV inverters can be oversized to allow more reactive power compensation capacity and the additional cost can be offset by the reduction of capacitor banks' investment [4]. The optimal energy management ability and the ancillary services supported by the PV based VPPs provide a potential to construct active distribution networks. Particularly, in short future, utilizing the PV based VPPs to support the VVC functions in the active distribution networks, improving power quality and reducing power losses, is inevitable.

1.2. Photovoltaic inverter reliability

With the rapid proliferation of PV systems in distribution networks, operational reliability issues come into the picture. The warranted lifetime of PV modules is about 20–30 years, whereas the lifetime of associated inverters is usually less than 15 years, and the number analyzed in 2012 was only around 5 years on average for PV inverters [5]. According to a study on the 5-year operating experience of a PV generation plant [6], the cost associated with PV inverter malfunctions takes 59% of the total system maintenance cost. Thus, the operational reliability of PV inverters is becoming one of the most crucial factors for the performance of the whole PV systems.

Power devices, e.g., insulated gate bipolar transistors (IGBTs) or metal-oxide-semiconductor field-effect transistors (MOSFETs) are the key power electronic components inside inverters. According to an industry-based survey [7], power devices are considered as one of the significantly fragile parts of inverters. Understanding failure mechanisms of power devices would be essential for the inverter reliability analysis. In addition, it is observed that the thermal cycling, i.e., the swings of junction temperature, is one of the most critical failure reasons for the power devices [8].

* Corresponding author.
E-mail address: cuo.zhang@unsw.edu.au (C. Zhang).

https://doi.org/10.1016/j.epsr.2020.106706
Received 4 October 2019; Received in revised form 17 March 2020; Accepted 1 August 2020
Available online 15 August 2020
0378-7796/

For the PV inverters, the lifetime of power devices is significantly affected by their operational conditions, which include control strategies, e.g., maximum power point tracking (MPPT) and reactive power compensation, as well as mission profiles including solar irradiance and ambient temperature. The reliability of PV systems under a MPPT algorithm is analyzed in [9] and an improved algorithm that can achieve a tradeoff between energy harvesting and lifetime consumption is proposed. Besides, the study in [10] indicates that both the PV active power outputs which are directly affected by solar irradiance and the ambient temperature have tremendous impacts on the lifetime of PV inverters. Thus, in order to predict the lifetime of PV inverters, both the control strategies and the mission profiles are expected to be taken into consideration. However, operational reliability of the PV inverters which are utilized for the VVC function has not been studied, leaving a research gap.

1.3. VVC and reliability analysis

As PV inverters can provide fast and flexible reactive power support with the marginal operating cost, the VVC based on the PV inverters is highly promising [11]. To achieve a VVC function, the inverters in the VPPs can be dispatched to support the optimal reactive power injection to the active distribution networks, aiming to minimize network power losses while keeping bus voltages within operating limits. It is worth noting that the reactive power compensation imposes additional operating burdens on the PV inverters, which have negative impacts on the inverter operational reliability in a long term. Thus, this issue leads to a significant thought whether the use of the inverters for the VVC function is economically efficient in the long run. In [12], the reliability of PV inverters under non-unity power factor operation and low-voltage ride-through is studied, but the reliability degradation rate and estimated lifetime of inverters are not specified. The operational reliability of PV inverters is analyzed in [13] and heavy lifetime degradation is identified due to reactive power compensation outside day-time feed-in hours. However, the analysis is conducted on a device level and only the functionality outside the feed-in hours is considered. In [14], a reactive power control scheme is proposed to stabilize the thermal fluctuation of power devices in wind farm, which indicates the potential positive impacts of reactive power on inverter reliability. Thus, it is imperative to further investigate the operational reliability of inverters which are coordinated for the VVC function on a system level.

In summary, utilization of PV inverters in VPPs to support the VVC function is highly promising for the stability and sustainability of modern power systems. However, the impacts of the additional VVC function on the inverter operational reliability have not been studied and addressed. Thus, this paper develops an inverter based VVC model considering uncertainties, a power loss model of the switch module considering the VVC results and a modified lifetime model based on Coffin-Manson model and manufacturing information. Last, with these models, this paper proposes an operational reliability assessment approach of PV inverters considering the VVC function. In case study, this approach is validated on a 33-bus distribution network, indicating the impacts of the additional VVC function on the inverter operational reliability and suggesting potential solutions.

2. Inverter based VVC under uncertainties

In order to analyze the inverter operational reliability considering the VVC function, firstly, an inverter based VVC optimization model under uncertainties such as PV power generation and load demand is developed in this section.

2.1. Inverter based VVC optimization model

The inverter based VVC optimization model aims to minimize the total network power losses while keeping bus voltages within allowed range, by optimizing the inverter reactive power outputs [15]. The inverter based VVC optimization model is formulated as follows:

$$\min_{q^g} \sum_{t\in T}\sum_{i\in I} P_{i,t}^{loss} \tag{1}$$

$$\text{s. t. } P_{i+1,t} = P_{i,t} + p_{i+1,t}^{g} - p_{i+1,t}^{l}, \ \forall\, i,\, t \tag{2}$$

$$Q_{i+1,t} = Q_{i,t} + q_{i+1,t}^{g} - q_{i+1,t}^{l}, \ \forall\, i,\, t \tag{3}$$

$$V_{i+1,t} = V_{i,t} - \frac{(r_i P_{i,t} + x_i Q_{i,t})}{V_0}, \forall\, i,\, t \tag{4}$$

$$P_{i,t}^{loss} = r_i \frac{P_{i,t}^2 + Q_{i,t}^2}{V_0^2}, \ \forall\, i,\, t \tag{5}$$

$$\underline{V}_i \le V_{i,t} \le \bar{V}_i, \ \forall\, i,\, t \tag{6}$$

$$-q_{i,t}^{max} \le q_{i,t}^{g} \le q_{i,t}^{max}, \ \forall\, i,\, t \tag{7}$$

$$(q_{i,t}^{max})^2 = (S_i)^2 - (p_{i,t}^{g})^2, \forall\, i,\, t \tag{8}$$

Objective function (1) aims to minimize the total network power loss over a given dispatch interval T by optimizing control variables, i.e., the inverter reactive power outputs q^g. Note that index t denotes each real time point in T and index i denotes the bus number in the bus set I. Eqs. (2)–(4) are the linearized DistFlow equations given by [11]. Herein, P_i and Q_i are active and reactive power flowing from bus i to $i+1$, p_i^l and q_i^l are active and reactive power demand at bus i, p_i^g and q_i^g represent active power generation and reactive power output of the PV systems at bus i, r_i and x_i represent resistance and reactance of the branch line between bus i and $i+1$, V_i is voltage magnitude of bus i and V_0 denotes voltage magnitude at the substation. Eq. (5) calculates power loss of each branch line. Constraints (6) and (7) ensure that bus voltage magnitude and inverter reactive power output of each bus are limited within the allowed ranges. Eq. (8) calculates real-time reactive power capacity of the inverters at each bus, where S_i denotes total apparent power capacity of the inverters at bus i.

The proposed VVC model (1)-(8) forms a quadratic programming problem containing uncertainty variables such as PV active power generation (p^g) and load demand (p^l and q^l).

2.2. Stochastic optimization method

To solve the VVC model that contains uncertainty variables, i.e., p^g, p^l and q^l, this paper applies a scenario-based stochastic optimization method.

The objective function of a scenario-based stochastic optimization model can be written as:

$$\min_{x} \sum_{s\in S} \rho_s G(x, \xi_s) \tag{9}$$

where x stands for the control variables, ξ_s denotes the uncertainty realization in scenario s, ρ_s represents the corresponding occurrence probability of scenario s and $G(x, \xi_s)$ is the objective function with the realized ξ_s.

Thus, the proposed VVC model can be converted as:

$$\min_{q^g} \sum_{s\in S} \rho_s \sum_{i\in I} P_{i,s}^{loss} \tag{10}$$

$$\text{s.t. (2)-(8)}, \forall i,\, s$$

$$\{(p_{i,s}^{g}, p_{i,s}^{l}, q_{i,s}^{l}), \rho_s\} \in \Psi_i, \ \forall\, i \tag{11}$$

where $p_{i,s}^g$, $p_{i,s}^l$ and $q_{i,s}^l$ represent the PV active power generation, active and reactive power demand in scenario s, and Ψ_i denotes the scenario set.

In this paper, Monte Carlo sampling (MCS) is used to generate the uncertainty realization scenarios with given probability density

functions (PDFs) which can characterize realization probability distribution. For example, Gaussian PDF, which can efficiently represent the uncertainty realization of PV outputs and loads, is applied in the MCS to construct the scenarios.

The proposed stochastic optimization problem of the VVC model can be solved by commercial solvers such as the GUROBI solver [16].

3. Inverter reliability assessment

With the VVC optimization model, the long-term inverter reactive power outputs can be simulated and obtained. Then the long-term operational reliability of the inverters considering the VVC function and the mission profiles (solar irradiance and ambient temperature) can be assessed. Firstly, a power loss model based on inverter active and reactive power outputs is developed to calculate the power losses dissipated in power devices inside the inverters. Herein, the active power outputs are affected by the solar irradiance and the reactive power outputs are optimized by the proposed VVC model under the uncertainties. Secondly, with the power losses, this paper applies the thermal model and one-year real-field data of ambient temperature to obtain the junction temperature profiles of the power devices. Then, a Rainflow counting technique [17] is used to interpret the randomly varying junction temperature profiles into regulated thermal cycles. Last, this paper modifies the Coffin-Manson model to estimate the lifetime of the power devices in the inverters with consideration of practical concerns.

3.1. Power loss model

In this paper, a single-phase PV inverter using IGBTs as power devices is used for operational reliability analysis. Since an IGBT module contains two parts, an IGBT unit and a diode unit, the power losses dissipated in these units are calculated separately.

3.1.1. IGBT power loss calculation

The power loss of the IGBT unit (P_S^{loss}) during one certain period can be expressed as:

$$P_S^{loss} = P_{S,con}^{loss} + P_{S,sw}^{loss} \tag{12}$$

where $P_{S,con}^{loss}$ and $P_{S,sw}^{loss}$ denote the conduction and switching losses of the IGBT unit, respectively. $P_{S,con}^{loss}$ and $P_{S,sw}^{loss}$ can be calculated by the following equations:

$$P_{S,con}^{loss} = \left(\frac{1}{2\pi} + \frac{m \times \cos\varphi}{8}\right) \times V_{CE0} \times i_P + \left(\frac{1}{8} + \frac{m \times \cos\varphi}{3\pi}\right) \times r_{CE} \times {i_P}^2 \tag{13}$$

$$P_{S,sw}^{loss} = \frac{f_{sw}}{\pi} \times (E_{on,nom} + E_{off,nom}) \times \frac{i_P \times V_{DC}}{I_{nom} \times V_{nom}} \tag{14}$$

where i_P denotes the inverter sinusoidal output current amplitude, V_{CE0} denotes the IGBT on-state zero-current collector-emitter voltage, r_{CE} denotes the IGBT on-state collector-emitter resistance, I_{nom}, V_{nom}, $E_{on,\ nom}$ and $E_{off,\ nom}$ denote the nominal current/voltage and the corresponding nominal single-pulse turn-on/off energy losses respectively, m denotes the PWM modulation rate, φ denotes the phase difference between modulation signal and inverter current, f_{sw} represents the switching frequency and V_{DC} denotes the applied DC link voltage.

3.1.2. Diode power loss caculation

The power loss dissipated on the diode unit can be calculated by:

$$P_D^{loss} = P_{D,con}^{loss} + P_{D,sw}^{loss} \tag{15}$$

$$P_{D,con}^{loss} = \left(\frac{1}{2\pi} - \frac{m \times \cos\varphi}{8}\right) \times V_{D0} \times i_P + \left(\frac{1}{8} - \frac{m \times \cos\varphi}{3\pi}\right) \times r_D \times {i_P}^2 \tag{16}$$

$$P_{D,sw}^{loss} = \frac{f_{sw}}{\pi} \times E_{rec,nom} \times \frac{i_P \times V_{DC}}{I_{nom} \times V_{nom}} \tag{17}$$

where P_D^{loss} denotes the power loss of the diode unit during one period, $P_{D,con}^{loss}$ and $P_{D,sw}^{loss}$ represent the conduction and switching power losses of the diode unit respectively, V_{D0} denotes the on-state zero-current voltage drop on the diode, r_D denotes the diode on-state resistance and $E_{rec,\ nom}$ represents the nominal value of single-pulse reverse recovery energy of the diode.

It is worth noting that generally, V_{CE0}, r_{CE}, V_{D0}, r_D, $E_{on,\ nom}$, $E_{off,\ nom}$, I_{nom}, V_{nom} and $E_{rec,\ nom}$ can be directly obtained from the IGBT manufacturer's datasheet. Thus, given the PWM modulation pulse patterns and the inverter DC link voltage, the total power loss of an IGBT module is a quadratic function of i_P.

3.1.3. Power loss calculation considering VVC function

As mentioned, the total power loss of an IGBT module has a close relationship with the sinusoidal output current amplitude i_P. For an inverter used to support the VVC function, i_P and cos φ can be calculated as follows:

$$i_P = \sqrt{2} \times \frac{\sqrt{(p^g)^2 + (q^g)^2}}{V_{AC}} \tag{18}$$

$$\cos\varphi = \frac{p^g}{\sqrt{(p^g)^2 + (q^g)^2}} \tag{19}$$

where p^g denotes the inverter active power output affected by the solar irradiance, q^g represents the inverter reactive power output determined by the VVC model, and V_{AC} denotes the inverter AC root mean square voltage. By substituting (18) and (19) into (12)-(17), the power loss model of an IGBT module considering inverter active and reactive power outputs can be obtained.

3.2. Thermal loading

3.2.1. Thermal model

The power losses dissipated in the power devices lead to junction temperature rise. Thus, an accurate thermal model of the IGBT module is required to transfer power losses into junction temperature fluctuations. In this paper, an IGBT thermal model based on Foster RC model as shown in Fig. 1 is developed. The junction temperature of the IGBT unit $T_{j,\ S}$ can be calculated as follows:

$$T_{j,S} = Z_{th,S(j-c)} \times P_S^{loss} + T_c \tag{20}$$

$$T_c = Z_{th,S(c-h)} \times P_S^{loss} + T_h \tag{21}$$

$$T_h = Z_{th(h-a)} \times \ (P_S^{loss} + P_D^{loss}) + T_a \tag{22}$$

where T_c and T_h denote the temperatures of the case and heatsink of the IGBT module, respectively, and T_a denotes the ambient temperature, $Z_{th(j-c)}$, $Z_{th(c-h)}$ and $Z_{th(h-a)}$ are the thermal impedances from junction to case, from case to heatsink and from heatsink to ambient, respectively.

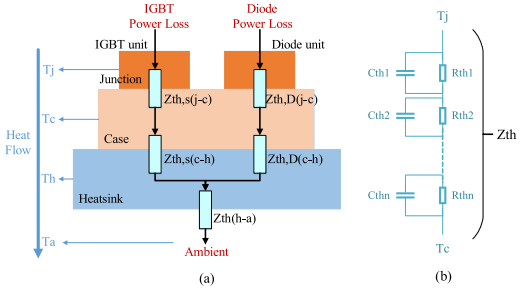

Fig. 1. IGBT thermal model. (a) Thermal structure of an IGBT module. (b) Foster RC thermal model.

The junction temperature of the IGBT unit can be obtained by:

$$T_{j,S} = (Z_{th,S(j-c)} + Z_{th,S(c-h)}) \times P_S^{loss} + Z_{th(h-a)} \times (P_S^{loss} + P_D^{loss}) + T_a. \quad (23)$$

Similarly, the junction temperature of the diode unit $T_{j,D}$ can be calculated as:

$$T_{j,D} = (Z_{th,D(j-c)} + Z_{th,D(c-h)}) \times P_D^{loss} + Z_{th(h-a)} \times (P_S^{loss} + P_D^{loss}) + T_a. \quad (24)$$

Note that the thermal capacitances in the applied thermal model only lead to fast thermal changes in time constants of milliseconds to seconds. For the long-term thermal analysis, the thermal capacitances can be ignored, and only the thermal resistances are taken into consideration [18].

3.2.2. Ambient temperature profile

Conventional reliability analysis usually focuses on the thermal loading and lifetime assessment under simple external conditions where the ambient temperature is assumed constant, which is not practical. Besides, it can be seen from (23) and (24) that the ambient temperature directly impacts on the IGBT and diode junction temperature. Thus, it is essential to have an accurate mission profile of ambient temperature for thermal loading analysis. Mission profiles of real-field ambient temperature are representative and often used for thermal loading analysis [19]. This paper applies an extensive real-field ambient temperature data for the long-term thermal loading analysis.

3.3. Thermal cycling interpretation

Due to irregular characteristics of the mission profiles, i.e., long-term PV outputs and ambient temperature, the obtained junction temperature profiles cannot follow repetitive patterns in terms of amplitude and duration. Thus, this paper applies a Rainflow counting method [17], which is a widely used cycle counting technique for stress analysis, to interpret the irregularly varying thermal loading into regulated thermal cycles. As a result, junction temperature variation ΔT_j, mean junction temperature T_{jm} and cycle heating period t_{on} of each regulated thermal cycle can be extracted for further lifetime estimation.

3.4. Lifetime estimation

Coffin-Manson model can be used for lifetime estimation of the power devices inside the inverters [20]. This model mainly describes the impact of the junction temperature variation ΔT_j on the lifetime, and it can be expressed as follows:

$$N_f = A \times (\Delta T_j)^{\alpha} \quad (25)$$

where N_f denotes the number of cycles to failure under the given ΔT_j, and A and α are constant coefficients.

The Coffin-Manson model is modified in [21] by adding the impact of the mean junction temperature T_{jm}, as:

$$N_f = A \times (\Delta T_j)^{\alpha} \times \exp\left(\frac{E_a}{k_B \times T_{jm}}\right) \quad (26)$$

where k_B is Boltzmann constant ($8.617 \times 10^{-5} eV \cdot K^{-1}$), and E_a denotes the activation energy, which is derived from extensive accelerated lifetime tests [22].

Furthermore, it is indicated in [23] that the thermal cycle heating period t_{on} can also significantly impact on the lifetime of the power devices.

On the other hand, lifetime models which are built on extensive lifetime test results done by the device manufacturers, are also widely adopted for lifetime estimation [18]. Thus, to consider the impacts of ΔT_j, T_{jm} as well as t_{on}, this paper proposes a modified lifetime model, combining the modified Coffin-Manson model in (26) and the manufacturer's application model in [24], as:

$$N_f = A \times (\Delta T_j)^{\alpha} \times \exp\left(\frac{E_a}{k_B \times T_{jm}}\right) \times \left(\frac{t_{on}}{t_{nom}}\right)^{-0.3} \quad (27)$$

where t_{nom} denotes the nominal cycle heating period, which is equal to 1.5 s. It is worth noting that the typical range of t_{on} adopted in [24] is from 0.1 s to 60 s. If used for longer cycles, the approximation can be applied based on the assumption that viscoplastic deformation saturates for time larger than 60 s.

Thus, N_f regarding certain ΔT_j, T_{jm} and t_{on} of each regulated cycle through the Rainflow counting is calculated by using (27). With the obtained N_f at each regulated cycle, Miner's rule [25] is applied to calculate the accumulated lifetime consumption LF_C of one mission profile duration T_{mp}, as:

$$LF_C = \sum_i \frac{n_i}{N_{fi}} \quad (28)$$

where i denotes the cycle number, n_i denotes the number of cycles accumulated for a certain ΔT_j, T_{jm} and t_{on}, and N_{fi} denotes the corresponding number of cycles to failure for the certain ΔT_j, T_{jm} and t_{on}. Thus, the final estimated lifetime of the IGBT modules can be obtained as:

$$LF = \frac{T_{mp}}{LF_C}. \quad (29)$$

4. Case study

4.1. Test system and parameter settings

In this paper, a 33-bus radial distribution network [26] is used to verify the proposed operational reliability assessment approach. This paper considers a high PV penetration case where 10 PV based VPPs are allocated at buses 6, 10, 13, 16, 17, 18, 21, 22, 25 and 30. Each VPP contains 100 individual PV systems of 5 kW and has the total PV power generation capacity of 500 kW. It is assumed that the inverter of each individual PV system is oversized by 10% to 5.5 kVA so as to provide more available reactive power compensation. The network topology with the VPPs is shown in Fig. 2. In this test, V_0 = 1p. u., and the allowed bus voltage range $[\underline{V}_i, \bar{V}_i]$ = [0.95, 1.05]p. u., the VVC dispatch interval is set at 1 hour, and the mission profile duration T_{mp} is one year. This paper assumes that all the inverters in a VPP share the same reactive power output amounts during each dispatch interval. It is also assumed that the network covers a relatively small area where the solar irradiance and the ambient temperature are identical at all the buses.

In this test, a 650-V/75-A IGBT module is used as the power device of the PV inverters. Parameters of this IGBT module can be found in [27]. PWM modulation rate m is set as 0.8, and switching frequency f_{sw}

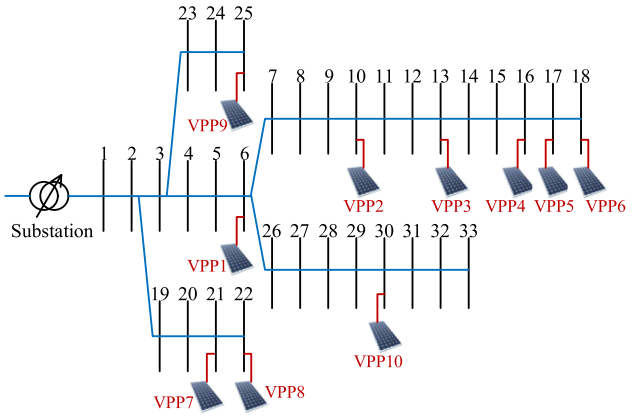

Fig. 2. Network topology of the test system.

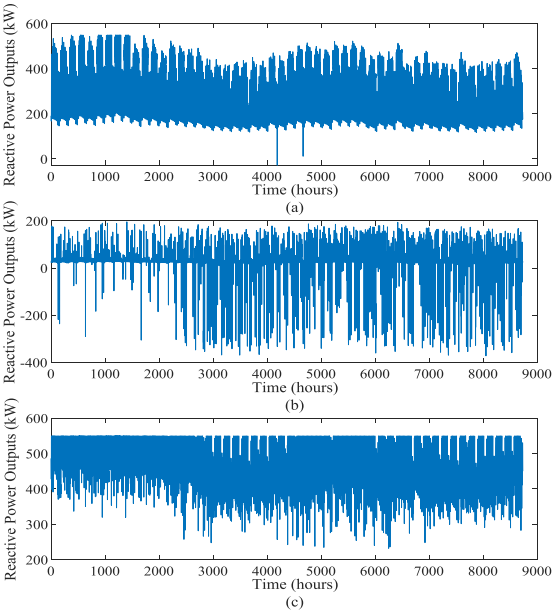

Fig. 3. One-year reactive power outputs of (a) VPP 1; (b) VPP 4; (c) VPP 10.

is 20 kHz. In this paper, according to [21, 24, 28], the activation energy E_a is set as $0.8eV$, and A and α are set as 4400 and -6.68, respectively.

Note that other systems, inverters and power devices can also be used without affecting the efficiency of the proposed operational reliability assessment approach.

4.2. VVC model simulation

In this paper, firstly, the PV power generation scenarios are constructed by the MCS with the Gaussian PDF based on historical solar irradiance profiles and the load scenarios are based on data of the IEEE Reliability Test System-1996 [29]. Then, the proposed inverter based VVC problem is solved by the stochastic optimization method (objective (10) subject to (2)-(8), (11)). The hourly dispatch results of each VPP for the whole year can be obtained. The inverter reactive power outputs of the VPPs 1, 4 and 10 are shown in Fig. 3. It is worth noting that positive values mean the VPP is injecting reactive power into the network while negative values for absorbing reactive power.

It can be seen that VPPs 1 and 10 are injecting reactive power the whole year, while VPP 4 is reducing reactive power injection and even absorbing reactive power during the midday peak PV generation periods.

4.3. Thermal loading and cycling results

To conduct the thermal loading analysis of inverters, a one-year mission profile of PV power generation and ambient temperature is needed. It is worth noting that the PV active power generation is based on the constructed PV output scenarios in the VVC model and the ambient temperature is based on the one-year hourly real-field data of Los Angeles from December 2016 to November 2017 [30].

With the mission profile, by applying the thermal model developed in Section III-*B*, the IGBT junction temperature profiles of the VPPs can be obtained, which are shown in Fig. 4. Junction temperature profiles without the VVC function are also obtained and shown for comparison in this figure. It can be seen that the junction temperatures of the IGBT modules increase due to the implementation of the VVC function. Moreover, VPP 10 has the largest temperature rise, but its temperature variation is smaller than that without the VVC function.

These junction temperature profiles can be further interpreted by the Rainflow counting method. It is worth noting that the junction

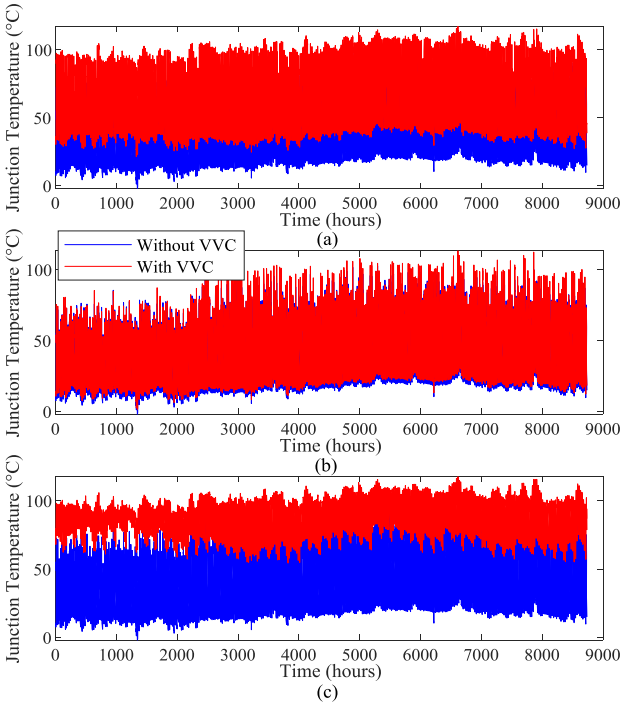

Fig. 4. One-year junction temperature profiles of the IGBT modules of (a) VPP 1; (b) VPP 4; (c) VPP 10.

temperature Rainflow counting results of all the VPPs are identical when not used for VVC function, due to the same mission profiles of PV power generation and ambient temperature at all buses. Taking the thermal loading of the IGBT modules in VPP 4 as an example, a total number of 4632 regulated thermal cycles are identified when used for the VVC function, and the corresponding ΔT_j, T_{jm} and t_{on} of each regulated cycle are obtained. Fig. 5 gives the Rainflow counting results of VPPs 1, 4 and 10 with and without the VVC function, which indicate the variations of ΔT_j and T_{jm} under the VVC case.

Fig. 6 gives a two-dementional demonstration of ΔT_j and T_{jm} to represent the difference between cases with and without VVC function. It can be seen that the implementation of VVC increases the mean junction temperature of VPPs 4 and 10, as well as the junction temperature variation of VPP 4. However, the jucntion temperature

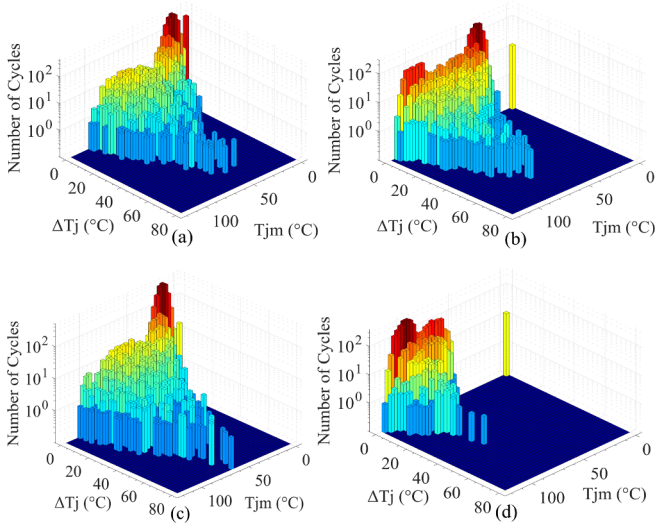

Fig. 5. Rainflow counting results of (a) VPPs without VVC; (b) VPP 1 with VVC; (c) VPP 4 with VVC; (d) VPP 10 with VVC.

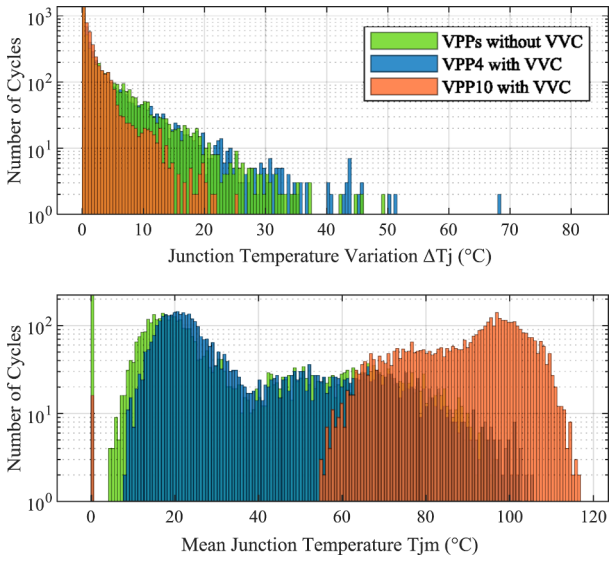

Fig. 6. Comparison of results of VPPs 4 and 10 under VVC case.

variation of VPP 10 is decreased.

4.4. Lifetime estimation results

With the Rainflow counting results, the estimated lifetime of the IGBT modules inside the PV inverters can be obtained by (27)-(29). Without the VVC function, the lifetime of all the inverters is calculated as a uniform 40.8 years, due to the identical mission profiles of PV active power outputs and ambient temperature. The estimated lifetime of all the inverters when used for the VVC function has been given in Table 1. Furthermore, the lifetime reduction percentages are also calculated and shown in the table. The negative percentages mean the lifetime increment rates.

The implementation of the inverter based VVC model reduces the lifetime of the inverters in VPPs 1, 3, 4, 5, 6, 8 and 9, whereas the other inverters have longer lifetime than that without the VVC function. It is worth noting that the inverters in VPP 4 have largest lifetime reduction, about 82.6% lifetime degradation, but the lifetime of the inverters in VPP 10 increases by about 6.3 times when used for the VVC function.

The Rainflow counting results of VPP 4 indicate larger mean junction temperature and junction temperature variation when used for the VVC function, which leads to significantly shortened lifetime. However, as for VPP 10, the junction temperature profile and the Rainflow counting results show that the implementation of the VVC function raises the mean junction temperature but reduces the junction temperature variation. This leads to the longer lifetime, indicating that in this simulation case, the lifetime degradation caused by junction temperature variation is larger than that by mean junction temperature.

In this test, the VVC reactive power output results are mainly impacted by the settings of network topology as well as the locations of VPPs. As for VPPs 4, 5 and 6, they have short lifetime. This is because they are densely located at the feeder end, and they need to absorb reactive power at peak power generation hours, which leads to significantly varying junction temperature. For VPP 10, it is the only VPP at its own feeder, so that it needs to constantly provide reactive power injection to the network. This leads to high mean junction temperature with low temperature variation, and then eventually leads to the extended lifetime. Thus, the simulation results provide useful insights on the impacts of VPP location on the inverter lifetime.

Table 1
Estimated lifetime of inverters.

VPP No.	1	2	3	4	5
Lifetime (years)	21.3	50.5	12.1	7.1	10.2
Reduction Percentage	47.8%	−23.8%	70.3%	82.6%	75%
VPP No.	6	7	8	9	10
Lifetime (years)	9.6	47.2	33.5	21	296.1
Reduction Percentage	76.5%	−15.7%	17.9%	48.5%	−625.7%

Table 2
Inverter lifetime (years) with different oversizing rates.

Oversizing Rate	VPP No. 1	2	3	4	5
5%	48.2	25.8	12.8	13.1	15.2
10%	21.3	50.5	12.1	7.1	10.2
20%	3.4	56.8	7.4	3.6	5.2
Oversizing Rate	VPP No. 6	7	8	9	10
5%	9.6	43.9	35.6	17.4	656.2
10%	9.6	47.2	33.5	21	296.1
20%	9.8	48.1	33.5	16.8	97.4

4.5. Reliability assessment with different oversizing rates

This section aims to explore the impacts of inverter oversizing rate on the inverter lifetime when used for the VVC function. Herein, the 5% and 20% inverter oversizing rates are also applied in the proposed VVC model. Note that other parameter settings are kept the same during the VVC optimization and reliability assessment processes. The simulation results regarding the different oversizing rates are given in Table 2.

It can be seen that the inverters' lifetime has high correlation with the oversizing rate. The lifetime of inverters in VPPs 1, 3, 4, 5 and 10 is decreased with the increasing oversizing rate. This indicates the oversizing of inverters at these buses has direct impacts on their reactive power output results during VVC process, which leads to high junction temperature variation or high mean junction temperature. Lifetime of inverters in VPPs 6, 7, 8 and 9 has minor changes, indicating the oversizing has less impacts on their VVC results. It is worth noting that there is a notable increase of inverter lifetime in VPP 2. Through analysis of the VVC simulation results, it is found that the reactive power outputs in VPP 2 are actually reduced due to the increased outputs of the oversized inverters at other buses.

It can be concluded that during VVC implementation, the inverter oversizing rate can have significant impacts on the inverter reliability and lifetime. The inverter oversizing is expected to be optimized considering the inverter reliability assessment in future works.

5. Conclusion and future works

This paper proposes an operational reliability assessment approach of PV inverters considering the VVC function. In this approach, with inverter based VVC results under the uncertainties, a power loss model and a thermal loading model of the inverter power devices are developed. Then, a modified lifetime estimation method based on the Coffin-Manson model is proposed. This approach is verified on a 33-bus radial distribution network.

The simulation results indicate that the implementation of the VVC function increases mean junction temperature but may decrease junction temperature variation, which may lead to positive or negative impacts on the lifetime of the power devices. Moreover, reliability assessment considering different inverter oversizing rates is conducted, which demonstrates high correlation between the inverter oversizing and its reliability. Thus, impacts of the VVC function on the inverter lifetime are expected to be considered with additional reliability constraints in the VVC optimization model, aiming to achieve a trade-off

between VVC performance and inverter long-term reliability.

In future works, inverter DC link voltage and corresponding constraints will be incorporated into the VVC optimization model, and advanced network power flow models such as the second order conic programming based branch flow model will be considered. Furthermore, the inverter reliability constraints will be developed and used in the VVC optimization model to guarantee both VVC performance and inverter lifetime.

Declaration of Competing Interest

The authors declare that they have no known competing financial interests or personal relationships that could have appeared to influence the work reported in this paper.

Acknowledgements

The work was supported in part by ARC Research Hub for Integrated Energy Storage Solutions (IH180100020) and in part by UNSW Digital Grid Futures Institute. The work of Q. Chai was supported by an Australian Government Research Training Program Scholarship.

References

[1] Australian PV Institute. Accessed: Sep. 2019. [On-Line]. Available:http://apvi.org.au.
[2] IEEE 1547 Standard for Interconnecting Distributed Resources With Electric Power Systems, 2019 [On-Line]. Available: http://grouper.ieee.org/groups/scc21/1547/1547_index.html accessed.
[3] EPRI, "Standard language protocols for photovoltaics and storage grid integration," Accessed: Jan. 2019. [Online]. Available:https://www.epri.com/#/pages/product/1020906/?lang=en-US.
[4] Y. Zhang, Y. Xu, H. Yang, Z. Dong, Voltage regulation-oriented co-planning of distributed generation and battery storage in active distribution networks, Int. J. Elec. Power Energy Syst. 105 (Feb.) (2019) 79–88.
[5] M. Schmela, PHOTON: inverter survey 2012 stats, Presentation at the PHOTON's 3rd PV Inverter Conference, San Francisco, 2012.
[6] L.M. Moore, H.N. Post, Five years of operating experience at a large, utility-scale photovoltaic generating plant, Prog. Photovolt: Res. Appl. 16 (3) (2008) 249–259.
[7] S. Yang, A.T. Bryant, P. A.Mawby, D. Xiang, L. Ran, P. Tavner, An industry-based survey of reliability in power electronic converters, IEEE Trans. Ind. Appl. 47 (May/Jun.(3)) (2011) 1441–1451.
[8] J. Due, S. Munk-Nielsen, R. Nielsen, Lifetime investigation of high power IGBT modules, Proc.14th Eur. Conf. Power Electron. Appl. Birmingham, England, 2011, pp. 1–8.
[9] M. Andresen, G. Buticchi, M. Liserre, Thermal stress analysis and MPPT optimization of photovoltaic systems, IEEE Trans. Ind. Electron. 63 (Aug.(8)) (2016) 4889–4898.
[10] M. Musallam, C. Yin, C. Bailey, M. Johnson, Mission profile-based reliability design and real-time life consumption estimation in power electronics, IEEE Trans. Power Electron. 30 (May(5)) (2015) 2601–2613.
[11] C. Zhang, Y. Xu, Z. Dong, J. Ravishankar, Three-stage robust inverter-based voltage/var control for distribution networks with high-level PV, IEEE Trans. Smart Grid. 10 (Jan.(1)) (2019) 782–793.
[12] J. Flicker, S. Gonzalez, Performance and reliability of PV inverter component and systems due to advanced inverter functionality, 2015 IEEE 42nd Photovoltaic Specialist Conference (PVSC), New Orleans, LA, 2015, pp. 1–5.
[13] A. Anurag, Y. Yang, F. Blaabjerg, Thermal performance and reliability analysis of single-phase PV inverters with reactive power injection outside feed-in operating hours, IEEE Trans. Emerg. Sel. Topics Power Electron. 3 (Dec.(4)) (2015) 870–880.
[14] K. Ma, M. Liserre, F. Blaabjerg, Reactive power influence on the thermal cycling of multi-mw wind power inverter, IEEE Trans. Ind. Appl. 49 (March-April(2)) (2013) 922–930.
[15] K. Turitsyn, P. Sulc, S. Backhaus, M. Chertkov, Options for control of reactive power by distributed photovoltaic generators, Proc. IEEE 99 (June(6)) (2011) 1063–1073.
[16] GUROBI. Accessed: Jul. 2019. [On-Line]. Available:http://www.gurobi.com.
[17] (2017), Standard Practices for Cycle Counting in Fatigue Analysis, West Conshohocken, PA, 2017 ASTM[On-Line]. Available: www.astm.org E1049-85 International.
[18] K. Ma, M. Liserre, F. Blaabjerg, T. Kerekes, Thermal loading and lifetime estimation for power device considering mission profiles in wind power converter, IEEE Trans. Power Electron. 30 (Feb.(2)) (2015) 590–602.
[19] P.D. Reigosa, H. Wang, Y. Yang, F. Blaabjerg, Prediction of bond wire fatigue of IGBTs in a PV inverter under a long-term operation, IEEE Trans. Power Electron. 31 (10) (Oct. 2016) 7171–7182.
[20] H. Huang, P.A. Mawby, A lifetime estimation technique for voltage source inverters, IEEE Trans. Power Electron. 28 (Aug.(8)) (2013) 4113–4119.
[21] M. Held, P. Jacob, G. Nicoletti, P. Scacco, M.H. Poech, Fast power cycling test of IGBT modules in traction application, Proc. Int. Conf. Power Electron. Drive Syst. Singapore, 1 1997, pp. 425–430.
[22] R. Moazzami, J.C. Lee, C. Hu, Temperature acceleration of time-dependent dielectric breakdown, IEEE Trans. Electron Devices 36 (Nov.(11)) (1989) 2462–2465.
[23] R. Bayerer, T. Herrmann, T. Licht, J. Lutz, M. Feller, Model for power cycling lifetime of IGBT modules - various factors influencing lifetime, Proc. Int. Conf. Integr. Power Electron. Syst. Nuremberg, Germany, 2008, pp. 1–6.
[24] Infineon Technologies AG, "PC and TC Diagrams," AN2019-05, Mar. 2019. [On-Line]. Available:https://www.infineon.com/dgdl/Infineon-AN2019-05_PC_and_TC_Diagrams-AN-v01_00-EN.pdf?fileId=5546d46269e1c019016a594443e4396b.
[25] M.A. Miner, Cumulative damage in fatigue, J. Appl. Mech. 12 (1945) A159–A164.
[26] M.E. Baran, F.F. Wu, Network reconfiguration in distribution systems for loss reduction and load balancing, IEEE Trans. Power Del. 4 (Apr.(2)) (1989) 1401–1407.
[27] Infineon Technologies AG, "Technical information," F4-75R07W2H3_B51 datasheet, Oct.2014.
[28] J. McPherson, Reliability Physics and Engineering, Springer Int, Switzerland, 2013.
[29] C. Grigg, The IEEE reliability test system-1996. a report prepared by the reliability test system task force of the application of probability methods subcommittee, IEEE Trans. Power Syst. 14 (Aug.(3)) (1999) 1010–1020.
[30] Kaggle Datasets, Historical Hourly Weather Data 2012-2017. Accessed: Jul. 2019. [On-Line]. Available:https://www.kaggle.com/selfishgene/historical-hourly-weather-data.